Supplementary information

Nanocrystalline Ni_5P_4: A hydrogen evolution electrocatalyst of exceptional efficiency in both alkaline and acidic media

Authors: A. B. Laursen, K. R. Patraju, M. J. Whitaker, M. Retuerto, T. Sarkar, N. Yao, K. V. Ramanujachary, M. Greenblatt, G. C. Dismukes

Contents

Experimental procedures

Catalyst synthesis

N.B.: pyrophoric white phosphorous is formed during synthesis and appropriate precautions should be taken. Only properly trained staff should perform these experiments, safety equipment such as goggles, lab coat and gloves (TOP aggressively attack butyl rubber gloves) are used at all times.

Ni_5P_4 nanoparticles (MPs): Ni_5P_4 MPs were synthesized by a procedure adapted from K. Ase et al[1]. In a typical synthesis 0.385 g Ni(acetylacetonate)$_2$·xH_2O, Ni(acac)$_2$ xH_2O (Sigma-Aldrich) was placed in a 3-necked flask together with 2.5 g tri-n-octylphosphine oxide, TOPO (Strem Chemicals). The flask was connected to a condenser in one port, a Schlenk line in the other, and pluged in the third. The condenser was connected to a silicone oil bubbler venting into a fume hood.

The flask was degassed under vacuum and then refilled with high purity Ar (Air-liquid). A flow of Ar was established through the flask before adding 10 ml of tri-n-octylphosphine, TOP (Strem Chemicals) under an Ar blanket. The solution was left under Ar flow for approximately 20 min to remove any introduced oxygen. The Ar flow was adjusted to a slow rate (1 bubble per second) and the flask was then placed on a pre-heated sand bath (Thermowell 500ml) at 390°C for 1.5 hr (solution temperature reaching 323-330°C). The TOPO quickly melted completely and the solution started refluxing and producing white smoke. It immediately turned brown, then black. The flask was buried so that the thermo probe of the temperature controller of the sand bath was level with the top of the reactant liquid and the sand surface was approximately 1 cm above the liquid level. N.B.: It was observed that if the reactant vessel was not buried deep enough in the sand, impurities of Ni_2P would appear in the PXRD pattern.

After reaction for 1.5 hr the flask was removed from the heat and cooled to room temperature. The black solution was transferred to a centrifuge tube with hexane (technical purity of hexane isomers) and diluted 4:10:1 by volume with 96% ethanol (EtOH) and acetic acid (98% Sigma-Aldrich). After centrifugation a gray powder was recovered. This powder was suspended in hexane by sonication and washed with addition of EtOH and acetic acid as above; this was repeated twice. The powder was then washed 3 times in acetone by centrifugation and decantation. The recovered powder was dried under vacuum.

Ni_2P NPs: Ni_2P NPs were synthesized according to the procedure by Muthuswamy et al[2]. In a typical synthesis 1.03 g Ni(acac)$_2$·xH_2O was placed in a 3-neck flask together with 10 ml n-octylether, and 4.6 g oleylamine. The flask was connected to a condenser and Schlenck line as for the procedure for Ni_5P_4 NPs. The flask was evacuated until bubbling subsided (about 10-15 min) then a flow of Ar was established and 10.2 ml TOP was added under an Ar blanket. The flask was then evacuated anew and heated lightly by placing 1 cm above a sand bath preheated to 230°C. The reagents dissolved under bubbling (water removal) and formed a deep green clear solution (approximately 30-60 min). Once all Ni(acac)$_2$ had dissolved and bubbling had subsided, the flask was filled with Ar and a slow Ar flow was established. The flask was placed in the preheated sand bath for 1 hr (at 230°C) during which a dark brown solution was obtained. The flask was placed so that the liquid level was flush with the sand level and the thermo probe was placed approximately midway between the sand surface and the bottom of the flask. N.B.: As for the Ni_5P_4 NP synthesis impurities were observed in the PXRD pattern if the flask was covered deeper in the sand bath.

After 1 hr of reaction the flask was removed from the sand bath, and the sand bath temperature was increased to 350°C. The flask was then re-inserted into the sand bath as described previously and reacted 3 hr. After reaction the flask was removed and allowed to cool to RT.

The Ni_2P NPs was recovered by centrifugation. The reaction solution was diluted 4:10 with acetone and centrifuged to obtain the precipitated particles. The particles were then washed 3 times by suspending in hexane and precipitating with acetone and acetic acid (4:10:1 by volume). Finally, the product was washed in EtOH and acetic acid (14:1 by volume). After drying in vacuum a black powder was recovered.

Ni_2P NP annealing: Prior to electrochemical tests the NP product was annealed in 5.04% H_2/Ar at 450°C for 30 min (ramp rate 5 K/min and hydrogen flow approx. 38 mL/min).

All chemicals were used as purchased and Nanopure water was used throughout. TOP was stored in an Ar glovebox and only removed just prior to use in sealed vials. TOPO was stored in a desiccator in air as it is hygroscopic but not air-sensitive.

All electrochemical glassware was cleaned in piranha (3:1 by volume 95-98% H_2SO_4 to 1% H_2O_2) prior to use. After measurements with Pt, the cell was cleaned in aqua regia then piranha. After acid cleaning the cell was rinsed in copious amounts of Nanopure water.

Powder X-ray Diffraction (PXRD)

PXRD analysis was performed on a Bruker AXS D8 Advance x-ray diffractometer with Cu $K\alpha_1$ radiation (1.54056 Å), a scan time of 1 hr or 12 hr, and a 2θ range of 15–70° or 10-120°. Samples were analyzed prior to electrochemical testing by dispersing the powder on a glass microscope slide and flattening the powder surface with another glass slide. Electrodes analyzed after electrochemical tests were measured by gently cutting the Ti-foil free from the Pyrex tube and removing the Cu-wire (*vide infra*). The pellet and Ti-foil was placed on a glass slide and the PXRD pattern recorded.

Data analysis was performed with the PAN'alytical High-Score software. For the full electrode assembly PXRD analysis shifts in peak positions were accounted for by shifting the most intense peaks of the Ni_5P_4 pattern. Phases were identified by comparison to the international crystal structure database (ICCD). Rietveld refinement of the annealed Ni_2P NPs was performed using the Fullproof software.

Electrode preparation

Ni_2P and Ni_5P_4: 50 mg of catalyst was pressed in a 6 mm die allowing the pressure to equilibrate at 2 tons for 10-15 min then increasing the pressure up to the final 4.5 ton. This pressure was held for 16 hr. After removing from the die, the pellet was quartered and each piece attached to a 6 mm diameter circular cut Ti-foil with Ag-paint (SPI supplies). After drying the Ti-foil and pellet was attached to a Cu-wire (curled into a spiral in one end) with Ag-paint. When the Ag-paint had cured (overnight at RT or 10 min at 120°C), the Cu-wire was threaded through a Pyrex glass tube (6 mm diameter). The non-conductive Loctite Hysol 1C epoxy was used to seal the Ti-foil to the glass tube and to cover the edges of the pellet leaving only the active electrode in contact with solution. After curing 3-4 hr at RT the epoxy was given the final cure at 120°C for 30 min. The electrode area was determined from a photo with the ImageJ software. After this procedure the electrode was rinsed in Nanopure water just prior to use.

After testing, the electrodes were removed quickly form the cell and rinsed immediately with water then EtOH. After this, the electrodes were stored until analyzed. When electrodes were re-used, they were gently cleaned with water just prior to use.

Pt: A Pt foil is sealed in a glass tube and sodded to a copper wire. The foil is etched until blank in aqua regia, then in piranha to remove traces of Cl^-. The foil is rinsed in copious amounts of Nanopure water and polished with 5 µm Al_2O_3, rinsed and sonicated in Nanopure water. The electrode is dried with a Kimwipe and masked with self-adhesive Teflon tape to expose a reduced area (0.016-0.092 cm^2).

Pt/C/Nafion: 6.8 mg 10 wt% Pt/C (Premetek) is dispersed in 0.5 mL Neutralized Nafion (1:2 by volume 5wt% Nafion (Sigma) in 0.1 M NaOH). The ink is sonicated for a minimum of 20 min prior to application. 5 µl of ink is drop-casted onto a 5 mm pre-polished (polished with 5 µm Al_2O_3 and sonicated in water) glassy carbon disc electrode, air dried for 1 hr, and cured at 120°C for 30 min. This gives a catalyst loading of 40.8 µg Pt/C per 0.196 cm^2.

Electrochemical setup

Electrochemical analyses were performed on a Princeton Advanced Research PARSTAT 2263 Advanced Electrochemical System potentiostat. A three-electrode dual compartment glass cell was used, except during gas-analysis measurements where a single compartment glass cell was used. The former allowed the working compartment to be stirred and purged with H_2, while minimizing crossover of O_2 from the counter electrode. The single compartment cell allowed the simultaneous collection of both product gasses without electrolyte diffusion between compartments due to the difference in pressure arising from the gas evolution in the anode vs. cathode compartment. Gas-analysis was performed in a two-electrode mode. Prior to measurements the glassware was cleaned in piranha then rinsed in copious amounts of water.

The counter electrode was a 1x1 cm boron-doped CVD diamond (B-doped diamond from Element six synthetic industrial diamonds) electrode contacted and encapsulated in a Loctite Hysol 1C epoxy analogous to the nickel phosphide pellet electrodes. The reference electrode was a Pine instrument Mini Ag/AgCl(KCl gel) electrode. The cell was continuously purged with N 4.5 H_2 (Airgas) during experiments, except for during gas product quantification by gas chromatography (GC) during which the cell was sealed. Prior to GC measurements the cell was purged in High purity Ar for 10-20 min, and the head space was measured by GC to be free from detectable amounts of O_2, N_2, or H_2 after this time.

All electrode potentials are reported vs. the reversible hydrogen electrode (RHE) and are thus corrected for pH as well as the reference electrode potential. The potential of the reference electrode vs. RHE was measured as the current curve intercept with 0 mA/cm^2 on a Pt disc electrode in both 1 M NaOH and 1 M H_2SO_4 ($E_{HER/HOR\ equilibrium}$), similarly to the method used by Shen et al.[3]. All measurements (except for the chronopotentiometric (CP) analysis) were additionally corrected for the solution IR-drop by measuring the electrochemical impedance spectrum (EIS) at small overpotentials with the Nyquist plot and determining the solution resistance ($R_{solution}$) from the first estimated intercept with the x-axis. $R_{solution}$ values ranged from 3-30 Ω. Corrections were made following the equation: $E[V] = E_{measured}[V] + 0.059\ V \cdot pH + E^{e}_{ref}[V] - I_{measured}[A] \cdot R_{solution}[\Omega] = E_{measured}[V] + E_{ref}[V] - I_{measured}[A] \cdot R_{solution}[\Omega]$.

HRTEM

High resolution electron microscopy imaging was recorded with a Philips CM200-FEG TEM (operating at 20 KeV, vacuum pressure of ~$2 \cdot 10^{-7}$ Torr) operated in the standard imaging and diffraction mode. The powder samples from the electrode were placed on a Au mesh TEM grid (300 mesh, 3 mm in diameter) covered by a thin carbon layer (support film). These samples were also analyzed with SEM. The instrument used was a FEI Quanta 200 FEG Environmental- Scanning Electron Microscope equipped with

an Oxford INCA Synergy 450 energy-dispersive X-ray microanalysis system, operated at 15 kV and 5 kV accelerating voltage, 140 pA probe current, 2,000 cps as average count rate on the whole spectrum, and a counting time of 60 s. The quantitative analysis on the final composition was determined by averaging 12 spectra from various regions of each sample.

Prior to microscopy, electrodes were run for 6 hr in either 1 M NaOH or 1 M H_2SO_4 under continuous H_2 bubbling, then quickly removed from the cell and rinsed in copious amounts of Nanopure water, then rinsed lightly in EtOH, and dried at RT. The solution exposed particles were removed by scratching the surface of the electrode lightly in a drop of high purity acetone. The acetone was then removed and dropped onto the sample grid and left to dry.

Supplementary data and discussion

Gas analysis

Gas determination was done on a PerkinElmer Clarus 680 Gas Chromatograph (GC) with a TCD detector. The column was kept at 40°C and Ar was used as the mobile phase; the resulting order of elution was H_2, O_2, and N_2. The H_2, N_2 and O_2 response are calibrated using pure reference gases. As there were always some air-leakage into the cell and from the injection needle, the amount of O_2 contributed by leaking was subtracted based on the N_2 signal with a 21% molar ratio of O_2 to N_2. The lower sensitivity towards O_2 as well as the peak overlap of the N_2 and O_2 signal reduced the accuracy of the determination of the Faradaic yield of O_2. 95% confidence intervals are given based on the student t-test analysis of data from 2 repetitions and 1-3 determinations per repetition.

Headspace samples were taken after running electrodes continuously at -1.96 mA for 3061 s, which was equivalent to 6 C of charge or approximately 0.76 ml H_2. This resulted in a current density that varied from -10 to -130 mA/cm^2 depending on the exact electrode area. This was done to avoid running the chamber for extended periods as the 16 hr CP analysis was observed to result in a significant amount of H_2 leaking from the cell; resulting in much reduced H_2 yields. The amount of H_2 leaked during a typical experiment was approximated by injecting 0.76 ml H_2 (equal to the amount of H_2 produced in a typical experiment) into the cell and measuring the amount left after the duration of a typical experiment. The amount of H_2 after ~70 min was found to be 104% ± 4%, this includes the estimated error of the volumetric H_2 addition. Based on this it is concluded that the leak rate in these experiments were negligible. To obtain the Faradaic yield during steady state condition the electrodes were conditioned for ~2 hr at -1.96 mA and the cell thoroughly degassed in Ar prior to gas evolution measurement. A similar measurement (without the preconditioning) was performed on the commercial Pt/C/Nafion control. The results are summarized in Table S 1 below.

Table S 1 Show Faradaic yields of H_2 and O_2 for the Ni_5P_4 and Pt/C/Nafion control

Catalyst	**pH 0**		**pH 14**	
	Faradaic H_2 yield	**Faradaic O_2 yield**	**Faradaic H_2 yield**	**Faradaic O_2 yield**
Ni_5P_4 MPs	92% ± 1%[1]	36% ± 3%[1]	93% ± 5%[1]	107% ± 3%[1]
Ni_2P NPs	Equal to Pt [3]	N/A	N/A	N/A
Pt/C/Nafion	89% ± 2%[1]	36% ± 6%[1]	89% ± 3%[1]	90% ± 4%[1]

1. 95% confidence interval based on student t-test.
2. The lower than unity O_2 yield in acid is attributed to counter electrode corrosion being preferred over the OER.
3. Measured by volumetric quantification see reference [4].

The Pt/C/Nafion samples produces basically (within 5%) faradaic yields of H_2 and O_2 1 M NaOH, however, in 1 M H_2SO_4 the faradaic H_2 yield is close to unity (within 9%) but the faradaic O_2 yield is only 36%. The significantly lower faradaic yield of O_2 for the Pt/C/Nafion in acid is attributed to the degradation of the counter electrode caused by the significant overpotential required for the OER in acidic solution on the poorly catalytic B-doped diamond surface. As our measurements does not allow for the detection of a CO_2 or CO gas product we cannot determine with absolute certainty where the corresponding charges went. However, as the faradaic H_2 yield is essentially unity we can preclude any H_2 consuming reactions (*e.g.* Oxygen Reduction Reaction and non-electrocatalytic water formation, back-reaction) causing the low faradaic O_2 yield. In summary, we can with less than 10% uncertainty determine that the faradaic H_2 yield is 100% in both 1 M H_2SO_4 and 1 M NaOH.

For the Ni_5P_4 samples the faradaic yield of H_2 was within the experimental error equal to that on Pt/C/Nafion verifying that the current at steady state is only due to the HER. These measurements also verify that H_2 is not consumed by back reaction (non-electrochemical water production) on the catalyst and that the O_2 Reduction Reaction (ORR) does not occur under these conditions.

Metal-ion leaching analysis

The concentration of Ni was followed during electrolysis experiments in the dual compartment three-electrode cell described above. This allowed minimal diffusion of oxygen from the counter electrode to the working electrode. The working compartment was furthermore purged with H_2 during catalysis to one maintain a constant 1 atm. of H_2 thus fixing the electrode potential of the HER and two to remove any O_2 diffusing from the counter compartment.

The working electrode is inserted into a pre-purged solution and the experiment started. The instrument introduces a lag-period here of approximately 1-2 min. for initialization before measuring CP analysis. During the CP analysis about 2-3mL of electrolyte is withdrawn from the working chamber a selected time periods. The volume left in the chamber after analysis was measured and from this and the volume of electrolyte withdrawn the concentration at each time point could be translated into the total Ni concentration. The working electrode chamber typically contained about 25-30 mL of electrolyte at the onset of the experiments.

The Ni ion concentration was detected by Inductive Couple Plasma – Optical Emission Spectroscopy (ICP-OES), the phosphate ion concentration could not be detected with this method. Prior to analysis the electrolyte sample was neutralized and brought to about 10% HNO_3 concentration by adding 560 µL concentrated 69-70% HNO_3 (J.T. Baker, ACS reagent) to 1.44 ml sample.

Ni concentration was measured at 3 characteristic wavelengths. The excellent agreement of these three measurements indicates the absence of matrix effects (see ICP OED Uncertainty/% in Table S 2 below).

Based on this 3 concentrations were calculated for each sample point and the averaged value is listed in Table S 2 below as the amount of Ni leached relative to the amount of Ni in the pellet exposed to electrolyte (see method for Turn-Over Frequency analysis below).

Sample to sample uncertainty is determined using the student t-test for the duplicates of time point 2 hours for the Ni_5P_4 MPs in acidic solution. The ~4% uncertainty obtained includes all preparation uncertainties and is about twice the 1-2% uncertainty attributable to the instrument accuracy in this matrix.

Table S 2 ICP-OES detected Ni concentration in electrolyte at selected times during 16 hr CP analysis. [a] Collected experimental uncertainty between replicated electrodes are determined at this time point as a 95% confidence interval using the student t-test. [b] ICP returned erroneous results for 2 out of 3 wavelengths at this time point, hence precluding the determination of the measurement uncertainty.

Ni_5P_4 in 1 M H_2SO_4

Time/[h]	Nickel in electrode/[mg]	Nickel dissolved/[mg]	Ni Leached/[%]	ICP-OES Uncertainty/[%]	Experimental Uncertainty/[%]
0	3.730439275	0.016347569	0.4%	0.7%	3.96
0.5	3.730439275	0.105276577	2.8%	0.8%	3.96
1	4.351956699	0.089472972	2.1%	N/A[b]	3.96
2[a]	3.730439275	0.154280152	4.1%	0.7%	3.96
2[a]	4.351956699	0.152888788	3.5%	1.5%	3.96
3	4.351956699	0.215365449	4.9%	1.5%	3.96
4	4.351956699	0.255337127	5.9%	1.2%	3.96
5	4.351956699	0.286518787	6.6%	1.1%	3.96
16	3.730439275	0.414673197	11.1%	1.4%	3.96
19	4.351956699	0.725065911	16.7%	0.7%	3.96

Ni_5P_4 in 1 M NaOH

Time/[h]	Nickel in electrode/[mg]	Nickel dissolved/[mg]	Ni Leached/[%]	ICP-OES Uncertainty/[%]	Experimental Uncertainty/[%]
0	5.098267009	0.003873661	0%	0.1%	3.96
0.5	5.098267009	0.003623292	0%	0.0%	3.96
2	5.098267009	0.002453423	0%	0.1%	3.96
16	5.098267009	0.002234463	0%	0.0%	3.96

Ni_2P in 1 M H_2SO_4

Time/[h]	Nickel in electrode/[mg]	Nickel dissolved/[mg]	Ni Leached/[%]	ICP-OES Uncertainty/[%]	Experimental Uncertainty/[%]
2	7.460497199	2.022259033	27.1%	0.4%	3.96
3	7.460497199	2.418591022	32.4%	0.7%	3.96
4	7.460497199	2.597373862	34.8%	0.7%	3.96
5	7.460497199	2.729151354	36.6%	1.3%	3.96
20	7.460497199	3.704198275	49.7%	2.3%	3.96

The time evolution of the nickel concentration in the electrolyte shows that in alkaline electrolyte none of the Ni dissolves as would be expected if there was a surface layer of $Ni_3(PO_4)_2$ on the particle surface. Nickel phosphates are not expected to dissolve at pH 14 but would be expected to dissolve in acids. Thus, it is no surprise that the Ni concentration increases immediately upon electrode insertion into the electrolyte. However, the concentration levels off at longer times indicating that the electrode is stable after the surface layer has been removed. The exponential fit of the Ni_5P_4 sample in acid levels off at

14.3% after about 16 hrs[1]. X. Hu and co-workers also observed a leveling off of the dissolution of Ni for their Ni_2P sample in 0.5 M H_2SO_4[5], although at a significantly lower total value. This behavior also explains the induction period of the Ni_5P_4 and Ni_2P in alkaline solution if the initial charge would be expected to go towards phosphate reduction into the parent phosphide. The difference in total Ni dissolution between this work and the study by Hu and co-workers are likely due to the passivation step the latter use prior to air-exposure—this would decrease the amount of phosphate formed and thus limit the dissolution in acid as well as the differences in electrode area, loading, and electrode design.

For a direct comparison under the experimental conditions used here, the dissolution of Ni from a Ni_2P NP electrode in 1 M H_2SO_4 was also monitored. It can clearly be seen that for this electrode about twice the final amount of Ni leached from Ni_5P_4 was dissolve at the first time point 2 hr. The exponential model used for Ni_5P_4 also fits this data showing that ~50.5% of Ni_2P NPs dissolve during catalysis, due to the limited number of time points at longer times the exact value of which the Ni_2P levels off could not be determined.

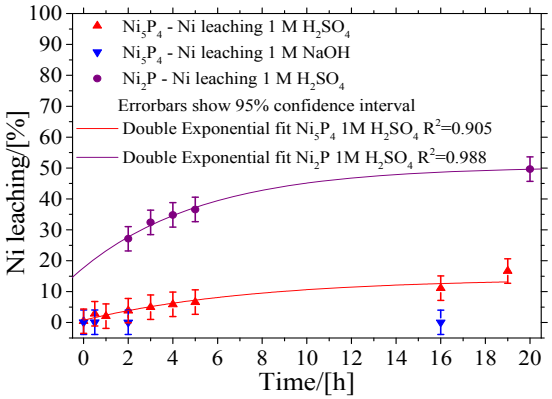

Fig. S 1 Ni leached from electrodes during a 20hr constant current measurement.

[1] The exponential fitting of the leaching of Ni from the Ni_2P and Ni_5P_4 was achieved by alternative locking the limiting value or the exponent and pre-exponent and then fitting the other. Fig. 4 (main manuscript) includes the R^2 value of the fit.

X-ray crystallographic analysis

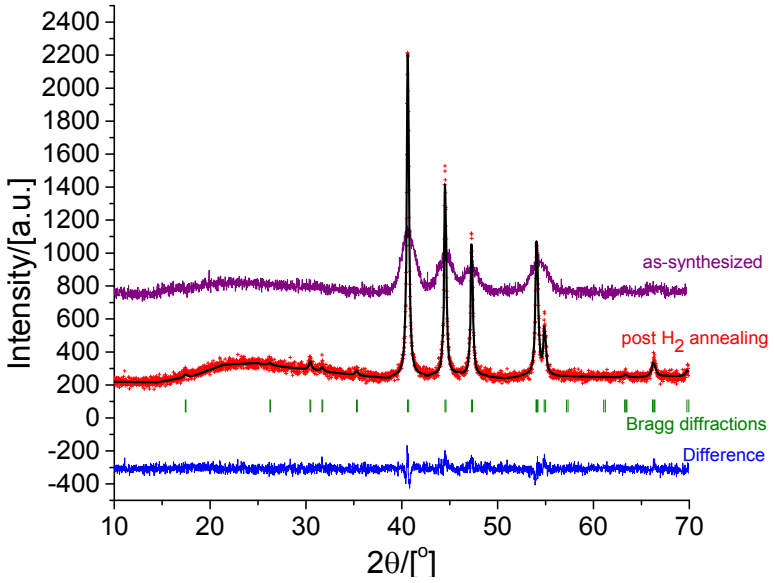

*Fig. S 2 PXRD analysis of Ni_2P sample as-synthesized (**purple**), after H_2 annealing (+ Exp & — calculated), difference (**blue**), and Bragg diffraction (**green**). Rietveld refinement was conducted on the Ni_2P NPs after annealing and the refinement used the Ni_2P reference pattern (PDF 03-065-3544), refining the following parameters: zero-point, scale factor, positional and thermal factors, and unit-cell parameters. Graphs are vertically displaced for clarity.*

Fig. S 2 show the PXRD patterns of the Ni_2P NPs sample as-synthesized and after the H_2 annealing at 450°C for 30 min as described by Popczun et al.[4]. The as-synthesized Ni_2P NPs show good agreement of the peak positions and intensities of the previously published reference structure and the annealed—verifying that the material is phase-pure Ni_2P and is unaltered by the annealing procedure. The annealed sample shows a higher degree of crystallinity (*vide infra*) and was thus used to confirm the structural purity using Rietveld refinement. The excellent agreement of the refinement shows that the Ni_2P sample is phase pure.

Applying the Scherrer equation to the as-synthesized Ni_2P nanoparticles we estimate the particle size to ~5nm; this is in good agreement with the N_2 BET surface area measurement of 69.4m^2/g as the latter corresponds to an average spherical particle diameter of 12nm. After the H_2 annealing the peaks has become significantly narrower indicating that the particles sinter significantly during annealing. A corresponding increase in the Scherrer equation derived particle size to 60nm was observed after annealing —indicating that the thermal treatment caused a significant amount of sintering.

A broad background peak is observed in both measurements, this stems from the glass sample holder. We also observed that the annealing causes a significant increased activity (data not shown), we attribute this to the removal of some surface residue from the synthesis remaining on the Ni_2P nanoparticles.

Fig. 1A in the main article shows the PXRD pattern of the Ni_5P_4 sample. The x-ray diffraction pattern was analyzed with the Rietveld method[6] using the refinement program Fullprof[7] and introducing microstructural effects to model the peak shape due to the small and irregular size of the crystals[8,9]. For the refinement of the profile we used a TCH pseudo-Voigt function to simulate the peak shape. In the final run the following parameters were refined: zero-point, scale factor, positional and thermal factors, preferential orientation, and unit-cell parameters.

For the microstructure analysis, an arbitrary shape of crystallites was simulated using an anisotropic size broadening treatment based in linear combinations of spherical harmonics; and finally for few individual reflections suffering from anomalous broadening or shift, we relaxed the peak broadening with respect to the instrumental resolution width, as well as the shift with respect to the calculated value of the peak position using the cell parameters. The resulting fit showed good reliability factors: χ^2= 4.17, R_p= 2.81%, R_{wp}= 3.69%, R_{exp}= 1.81%, demonstrating that the product is indeed phase-pure nanocrystals of Ni_5P_4.

The Scherrer equation results in a crystallite size of ~20 nm. The measured BET surface area of <1 m^2/g indicate a particle size of <0.95 µm assuming spherical particles in reasonable agreement with the HRTEM analysis (see *vide infra*).

Fig. S 3 shows PXRD measurements on 3 pellet electrodes exposed to a 2 hr CP analysis in 1 M NaOH or 1 M H_2SO_4 and a pristine electrode without exposure to electrolyte. Due to the very small electrode area ~0.03–0.1 cm^2 the scan time for these experiments is increased to 12 hr—even still the signal to noise ratio is quite low. This low signal complicates the assignment of diffraction peaks to phases—however a few peaks could be seen in all samples. The large broad peak centered at ~23° most likely stems from the amorphous glass sample holder. The physical height of the electrodes off sets the 2θ axis and the spectra are manually aligned to the most intense peak (Ni_5P_4 (214) at 2θ = 52.979°). The main lines for the Ni_5P_4 phase could also be identified in all three samples. In addition to these peaks a few new peaks could tentatively be discerned in the patterns, the peaks at 27.0° and 60.8° are particularly intense. These peak are present not only in the two CP analyzed samples but also in the pristine samples, so they must be ascribed to the electrode assembly (most likely the epoxy coating). Indeed, all of the peaks (significant over the noise level) not attributable to the Ni_5P_4 could be found in all three samples indicating that they all originate from the electrode assembly. Within the limit of detection the PXRD patterns before and after 2 hr CP analysis corroborate the conclusions from HRTEM, SEM and SEM-EDXS that Ni_5P_4 is the only crystalline phase present before and after catalytic H_2 evolution.

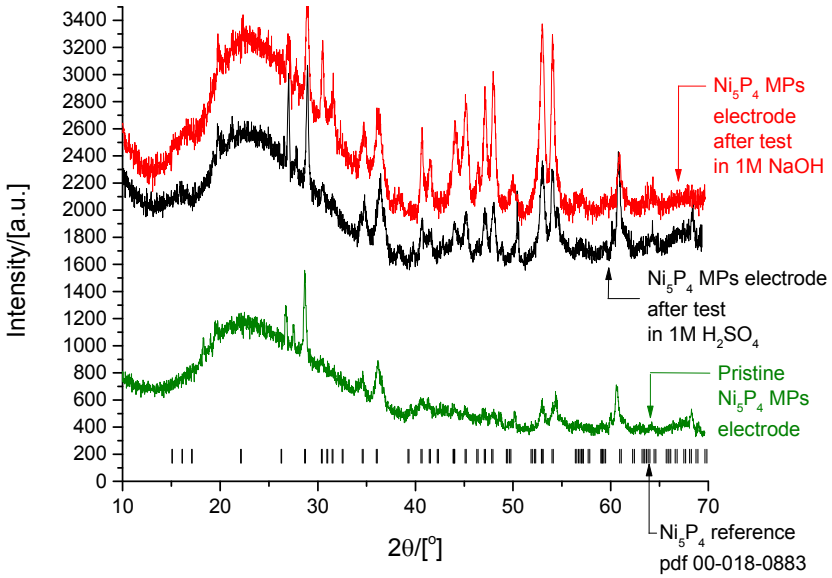

*Fig. S 3 PXRD pattern of 3 Ni_5P_4 pellet electrodes exposed to (**red**) CP analysis 2 hr in 1 M NaOH, (**black**) CP analysis 2 hr in 1 M H_2SO_4, and (**green**) a pristine electrode without electrolyte exposure. Scan time is 12 hr for increased resolution.*

Electrochemical analysis

Cyclic voltammetry (CV) analysis

CV data for the Ni_5P_4 pellets is performed after holding the electrodes at a reducing potential of approximately -0.43 V vs. RHE for 1 hr before performing cyclic voltammetry(CV) at 1 mV/sec in the potential region of -0.43 – +0.02 V vs. RHE starting from the negative potential. This was done to reduce the capacitive feature (at low overpotentials) in the CVs to a minimum. In addition, the Ni_5P_4 pellets were pre-conditioned by holding at a steady -10 mA/cm^2 for 16 hr, this was done to eliminate the initial feature seen in the CP (see Fig. 3C in main article). For the Ni_2P pellets a significant decomposition is observed during the catalytic reaction (see Fig. 3D in main article), thus pristine pellets are measured in this case. The decomposition of the Ni_2P phase is in agreement with the observations of Popczun et al[4]. The activity of the bulk Pt electrode is measured on a pristine electrode as well due to the slow decrease observed in the CP analysis (see Fig. 3C in main article), to minimize the effects of impurities the Pt electrode is scanned to 1.35 V vs RHE which should anodically remove any impurities.

CV data is furthermore averaged over the forward and backward scans to eliminate the residual capacitive features. Fig. S 4 shows two scans on a Ni_5P_4 MPs, Ni_2P NPs, and Pt electrode as well as the average scan shown in Fig. 3A and B.

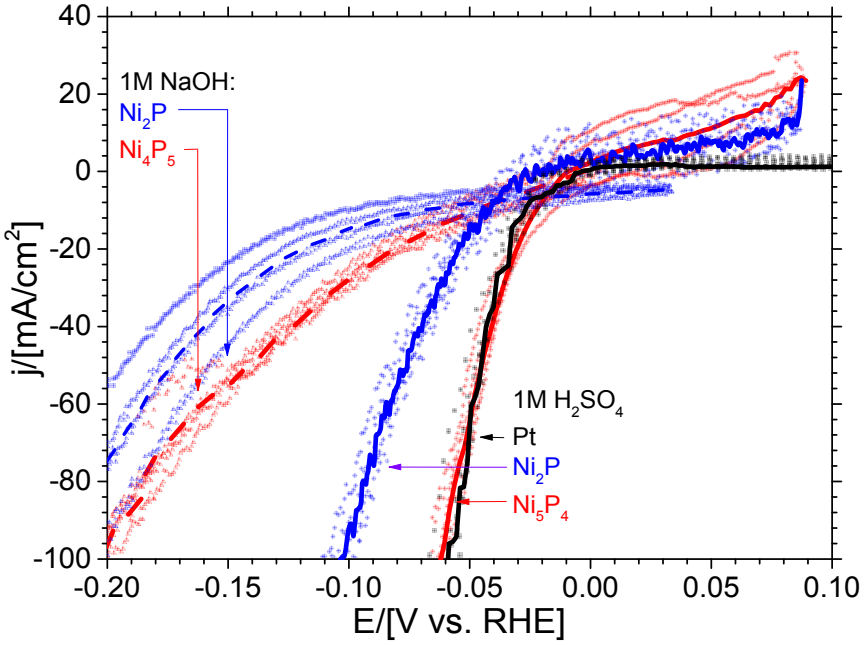

Fig. S 4 Raw CV data and averaged curves from Fig. 2A. Showing the large capacitive features at low overpotentials on the Ni_2P and Ni_5P_4 pellet electrodes.

Fig. S 5 below shows the effect of IR drop correction. The effect is seen to be minimal at these current densities due to the small electrode surface area and fairly small IR drop resistances (3-30Ω).

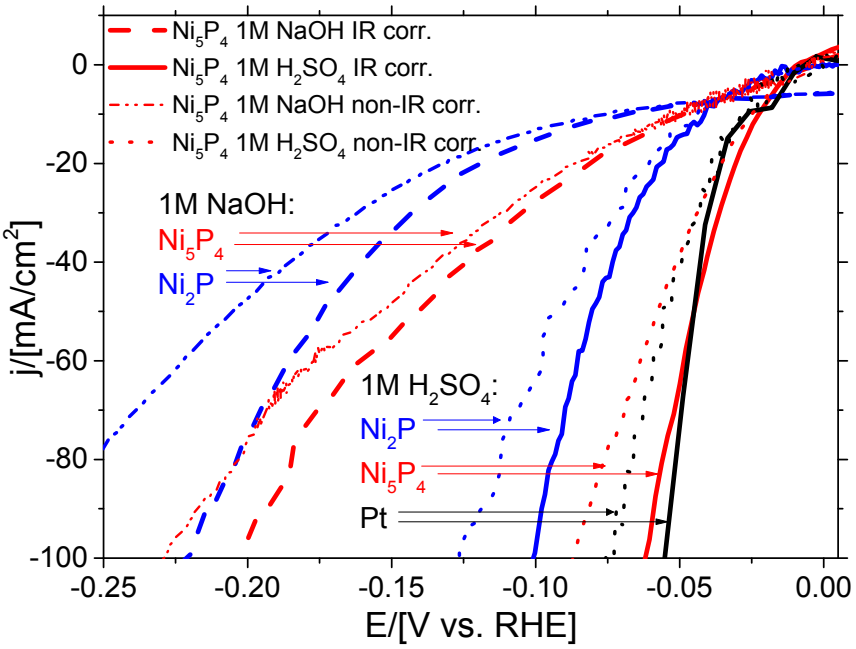

Fig. S 5 shows the averaged CV data before and after uncompensated IR drop correction.

Tafel analysis

Tafel analysis is performed on the CV data recorded as described above. To average out the capacitive feature on the pellet electrodes only the averaged (over forward and backward scan) data was processed. Data was further truncated to exclude the positive (oxidative) current data points.

According to the guidelines given by Bard and Faulkner[10] the Tafel analysis should be valid at overpotentials where the reverse current (HOR) is less than 1% of the forward current (HER). This equals a minimal required overpotential of half the obtained Tafel slope[3]. This requirement was followed in the analyses.

Fig. S5-8 also shows the Tafel analyses for the Ni_2P, Pt and Ni_5P_4 electrodes.

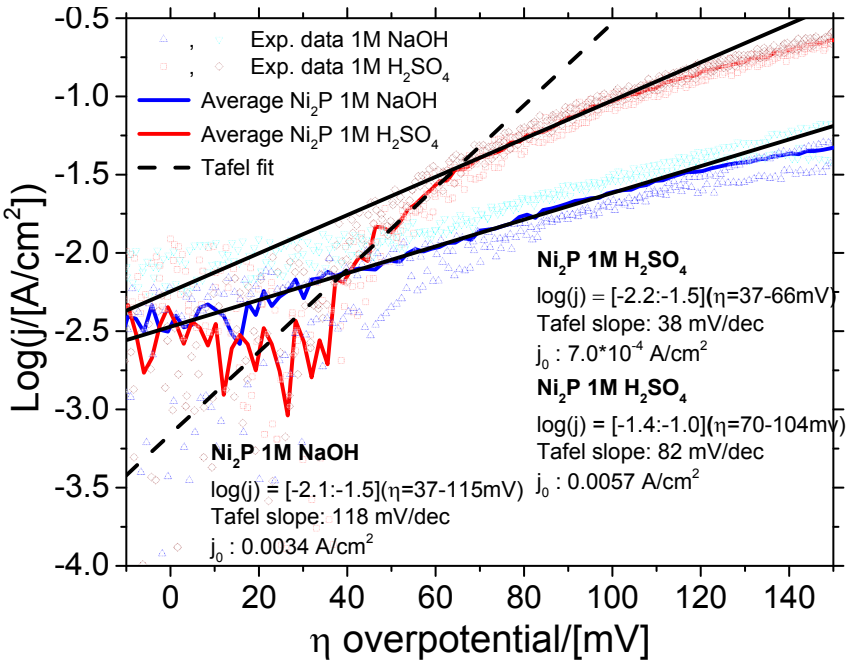

Fig. S 6 shows the Tafel analysis for Ni_2P. CVs are obtained for fresh electrodes to avoid effects of the decomposition of Ni_2P in the Tafel analysis. Scan rate 1 mV/s under 1 atm. H_2. Data is IR-drop corrected.

The Tafel analysis of the Ni_2P NPs, seen above in Fig. S 6, shows two Tafel regions at low pH. The Tafel slope at low current densities (covering 0.7 decades) is 38 mV/dec and the corresponding exchange current density is measured to be $j_0 = 7.0 \cdot 10^{-4}$ A/cm^2, at higher current densities (covering 0.3 decades) the Tafel slope increases to 82 mV/dec, likely due to the onset of diffusion limitations. These values should be compared to the low current density Tafel slope of 47 mV/dec, $j_0 = 3.3 \cdot 10^{-5}$ A/cm^2 and high current density Tafel slope of 81 mV/dec, reported in the literature[1]. The low current density Tafel slope observed in this work is smaller than that in literature and the corresponding exchange current density is larger by about a factor of two. This improvement is a sign that the HER kinetics measured on the pellet electrodes tested here are not limited by the same mechanism, indicating that the thin film electrodes tested by Popczun et al.[4] were limited by another and slower rate determining step than the pellet electrodes here. This could indicate that the thin film electrodes were limited by a low loading (too few active sites) or the higher pH used by Popczun et al.[4] (1 M H_2SO_4 vs. 0.5 M H_2SO_4) at low current densities. The Tafel slope at higher current densities corresponds well to that expected from literature. These measurements indicates that the activity of the Ni_2P NPs synthesized in this work are equivalent to the ones recently reported by Popczun et al.[4] and that the difference observed at low currents does not apply at higher currents. Under alkaline conditions only one Tafel slope of 118 mV/dec is observed (measured over 0.6 decades) with a corresponding exchange current density of $j_0 = 3.4 \cdot 10^{-3}$ A/cm^2.

These differences in kinetics between what is observed here and in Ref. 3 at low current densities, means that the Ni_2P NP electrode performs better as a pressed pellet than as drop-cast thin-film. Thus, to obtain j = -20 mA/cm^2 -0.055 V vs. RHE (1 M H_2SO_4) must be applied—less than half of the -0.130 V (0.5 M H_2SO_4) reported previosuly[1]. Interestingly, the discrepancy is even greater in alkaline solution, -0.088 V vs. RHE compared to -0.205 V vs. RHE[1]. We ascribe the discrepancy to the higher loading of catalyst in the pellets and the larger surface area in the material tested here (69.4 m^2/g vs. 32.8 m^2/g[1]).

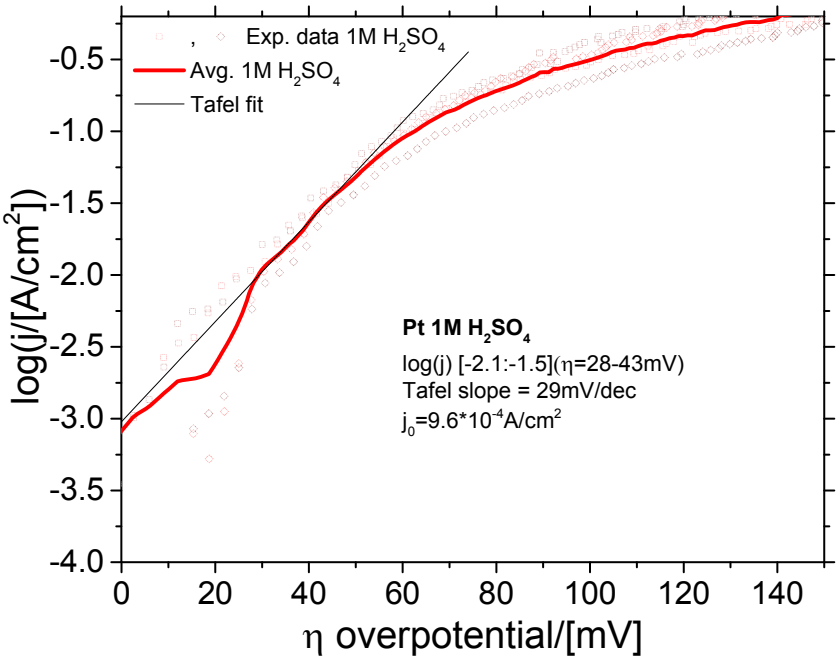

Fig. S 7 Tafel analysis for a bulk Pt foil electrode in 1 M H_2SO_4 and 1 M NaOH under 1 atm. of H_2. Scan rate 1 mV/s. IR-drop is corrected.

The archetypical HER catalyst is Pt and has been studied in great detail. Due to the micrometer size of the Ni_5P_4 MP agglomerates we compare their activity to a Pt foil electrode. The observed potential required for j = -10 mA/cm^2 on Pt in 1 M H_2SO_4 is -27 mV vs. RHE, respectively. As discussed above the region of Tafel analysis is the first linear region of current density covering around half to one order of magnitude, this is limited from the normally recommended one to two orders because measurements are done on a stationary electrode. The resulting Tafel slope is 29 mV/dec in 1 M H_2SO_4, the exchange current density (j_0) is $9.6 \cdot 10^{-4}$ A/cm^2 in 1 M H_2SO_4. The Tafel slopes are close to the 29.5 mV/dec Tafel slope reported for Pt(polycrystalline) in 0.5 M H_2SO_4 [3]. The exchange current density, $j_o = 9.6 \cdot 10^{-4}$ A/cm^2 is in the $1 \cdot 10^{-4}$ to $10 \cdot 10^{-4}$ A/cm^2 range reported in literature[3]. At higher current densities the Tafel slope for Pt in begins to deviate from the above reported values. This is likely due to the onset of transport limitations. As the solution is only stirred, transport effects are expected to contribute to the Tafel slope at fairly low current densities, as opposed to measurements on a rotating disc setup where these can be eliminated.

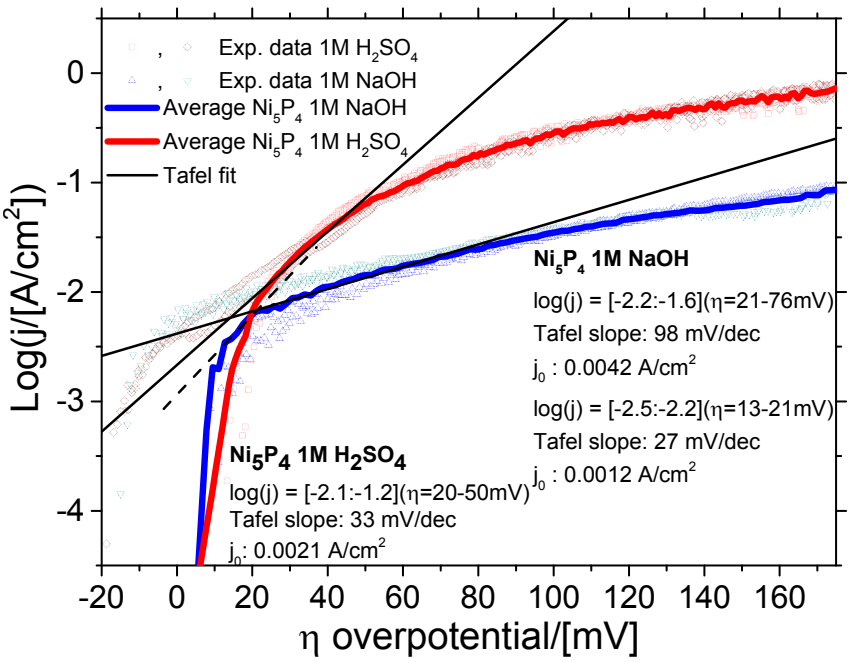

Fig. S 8 Tafel and onset potential analysis for Ni_5P_4 MPs in 1 M H_2SO_4 and 1M NaOH under 1 atm. of H_2. Samples are held at -480 mV for 1 hr before sweeping the potential positive for the first CV cycle. This is done to ensure that the measured kinetics are from the steady state active catalyst. Samples have been pre-conditioned at -10 mA/cm^2 for 16 hr prior to these measurements.

For the Ni_5P_4 MP electrodes, the sample is initially pre-conditioned by CP measurement at -10 mA/cm^2 for 16 hr. The electrode is rinsed in water then acetone and dried at RT. The electrode is then immersed in fresh electrolyte in a 2-compartment cell as described previously. The cell is then purged with H_2 before the experiment is started. The experiment includes a 1 hr CA (constant potential) conditioning at approximately -430 mV vs. RHE. After the conditioning the sample is scanned at 1 mV/s for 2 cycles. The open symbols in Fig. S 8 indicate the recorded data points, the full line is the averaged curve over the 2 cycles. Tafel analysis is performed on the averaged data points. For the Ni_5P_4 MP sample in 1 M NaOH it is observed that the initial Tafel slope of 27 mV/dec only covers 0.4 decades; after this the Tafel slope increases to 98 mV/dec. The change in Tafel slope was verified by taking the 1'st derivative, the overpotential corresponding to this change is determined to be 20 mV, in agreement with the above Tafel analysis. The two different Tafel slopes we attribute to the onset of diffusion limitations in the alkaline conditions, as these measurements are performed under stirring, but not on a rotating disc setup, where transport effects can be avoided in a wider potential interval. In acid, the Tafel slope for the Ni_5P_4 MP electrode is only 33 mV, which is comparable to that of Pt; this Tafel region stretches 0.9 decades of current density before it begins to deviate—this is again attributed to the onset of diffusion limitations. The deviation between the averaged curve and the individual measurement gives the appearance of a continuously changing Tafel slope; however as we could obtain a linear fit over almost a full decade, it is believed that the measured Tafel slope is correct within the uncertainty of the measurement. Further studies of this material on rotating disc electrodes are currently under way.

Chronopotentiometry

Chronopotentiometric (CP) analysis of Ni_5P_4, Ni_2P and Pt at -10 mA/cm^2.

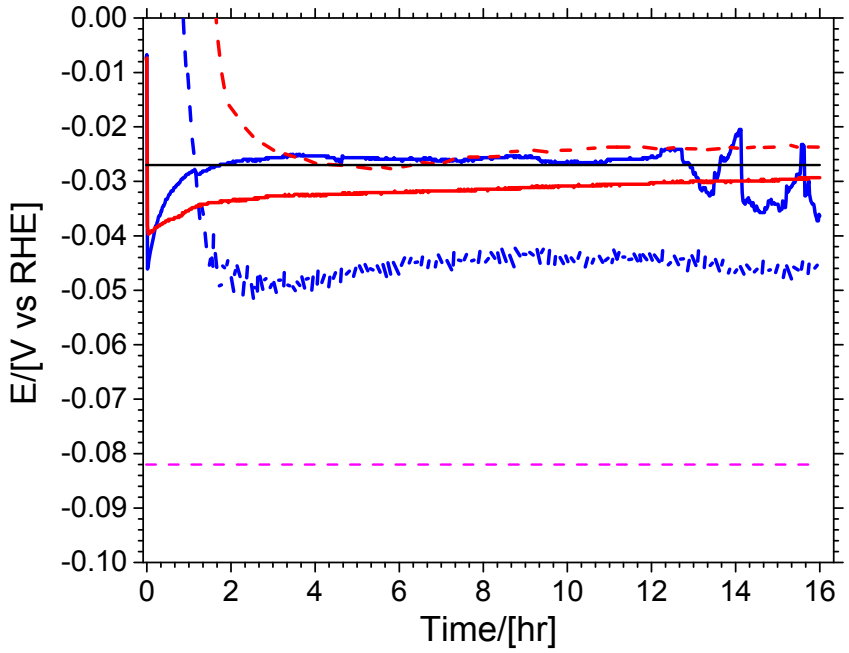

*Fig. S 9 CP analysis of Ni_5P_4 MPs (**red**), Ni_2P NPs (**blue**) in 1 M H_2SO_4 (solid line) and 1 M NaOH (dashed line). The kinetic potential for -10 mA/cm^2 for Pt in 1 M H_2SO_4 and NiMo NPs (**magenta**) in 1 M NaOH.*

Ni_2P NPs and Ni_5P_4 MPs show potentials positive of the thermodynamically allowed for H_2 evolution at times <3 hr in alkaline electrolyte. The required potential increases with time until a steady state level is reached at potentials negative of the thermodynamic limit. This induction period would indicate that an initial reduction reaction is occurring. As the structure and composition—as determined by HRTEM and SEM-EDXS—after 6 hr of electrolysis is in agreement with the standard data for Ni_5P_4 this induction period is not likely to affect the crystal structure or composition. It must therefore be assumed that this induction period corresponds to a surface reduction.

In contrast to this behavior the nickel phosphides in acid show a decrease in required overpotential for -10 mA/cm^2 within the first ~2 hr. This would be consistent with an initial reduction resulting in an improved conduction through the catalyst pellet. This induction is clearly pH dependent, and is under further investigation.

For comparison the potential required for j = -10 mA/cm^2 for Pt in 1 M H_2SO_4 (this work) and NiMo alloy NPs[11] in alkali

Turn-over frequency analysis

To estimate the turn-over frequency (TOF) as a function of overpotential, the number of surface atoms per surface area of the particles are determined.

We employed the method proposed by E. J. Popczun et al.[4] This method is a crude upper bound approximation, which averages the atoms in the molar volume to a surface assuming a cubic unit cell. The data for this analysis is taken from the PXRD reference patterns (Ni_5P_4 PDF 00-018-0883, Ni_2P 03-065-3544, and Pt 00-004-0802). Below is given an example for Ni_5P_4 MPs and this procedure is then applied similarly to Ni_2P NPs and Pt.

Ni_5P_4:

The hexagonal unit cell has a molar volume of:

$$V_m = F_w/\rho = \frac{417.36 g/mol}{6.32 g/cm^3} = 66.0038\ cm^3/mol_{Ni_5P_4}$$

Each formula unit contains 9 atoms of Ni and P. The average surface occupancy thus becomes:

$$\left(\frac{9\ atoms/formula\ unit}{\frac{66.038\ cm^3/mol_{Ni_5P_4}}{6.0221 \cdot 10^{23} mol^{-1}}}\right)^{2/3} = 1.89 \cdot 10^{15}\ surface\ atoms/cm^2$$

Similarly, the number for Ni_2P is calculated as: $2.00 \cdot 10^{15}$ surface atoms/cm^2 and for Pt $4.13 \cdot 10^{15}$ atoms/cm^2

The N_2 BET surface area of Ni_5P_4 <1 m^2/g (as the surface area is too low for accurate determination, 1 m^2/g is as an upper bound surface area in the following), Ni_2P 69.4 m^2/g (prior to H_2 annealing). For the Pt electrode a completely smooth electrode surface is leading to an upper limit estimate of the Pt TOF. In addition, we evaluated a Pt/C/Nafion composite electrode with a well-known surface area of Pt: 12 m^2 Pt/g catalyst (manufacturer's data sheet). Using the above estimations the number of surface atoms in each sample may be approximated.

Alternatively, the electrochemical surface area may be determined by electrochemical methods. However, this is only accurate relative to a non-porous reference or in a homologous series of electrochemically active compounds. Unfortunately, such a reference does not exists for the nickel phosphides limiting this method's applicability.

To estimate the exposed area for the pellet electrodes an upper limit is chosen. In this approximation we assume that the amount of catalyst loaded below the exposed surface is all in contact with the electrolyte. This will overestimate the active area, but the exposed surface could not be obtained from the available data. As each electrode consists of an irregular piece from a pressed 6 mm disc, we multiply the exposed geometric surface area with, $\frac{50\ \mathrm{mg}}{\left(\frac{0.6\ \mathrm{cm}}{2}\right)^2 \cdot \pi}$, to get the mass loading of the electrode. This is then multiplied with the BET surface area and number of surface atoms/cm^2. The resulting active areas for representative electrodes become:

Table S 3 Catalyst physical properties. Table shows the geometric surface area, the corresponding mass loading and estimated active number of surface atoms.

Catalyst	geometric surface area/[cm^2]	Mass loading /[g]	BET surface area/[m^2/g]	Estimated surface atoms /[cm^{-2}]	Active surface atoms /[moles]
Ni_2P	0.066	$1.17 \cdot 10^{-2}$	69.4	$2.00 \cdot 10^{15}$	$2.69 \cdot 10^{-5}$
10% Pt/C	0.196	$4.08 \cdot 10^{-6}$	12	$4.13 \cdot 10^{15}$	$3.36 \cdot 10^{-9}$
Bulk Pt	0.092	N/A	N/A	$4.13 \cdot 10^{15}$	$6.30 \cdot 10^{-10}$
Ni_5P_4	0.064	$1.13 \cdot 10^{-2}$	1	$1.89 \cdot 10^{15}$	$3.55 \cdot 10^{-7}$

We then recalculate the currents in the CVs to moles of H_2 and divide with the moles of active surface atoms. Fig. S 10 shows the resulting TOF vs. applied potentials. It may be seen that due to the high efficiency the Pt this sample has about 1-2 orders of magnitude larger activity than Ni_5P_4 MPs. When zoomed in further the TOF of Ni_2P NPs are seen to be approximately 2 orders of magnitude smaller than for Ni_5P_4 MPs.

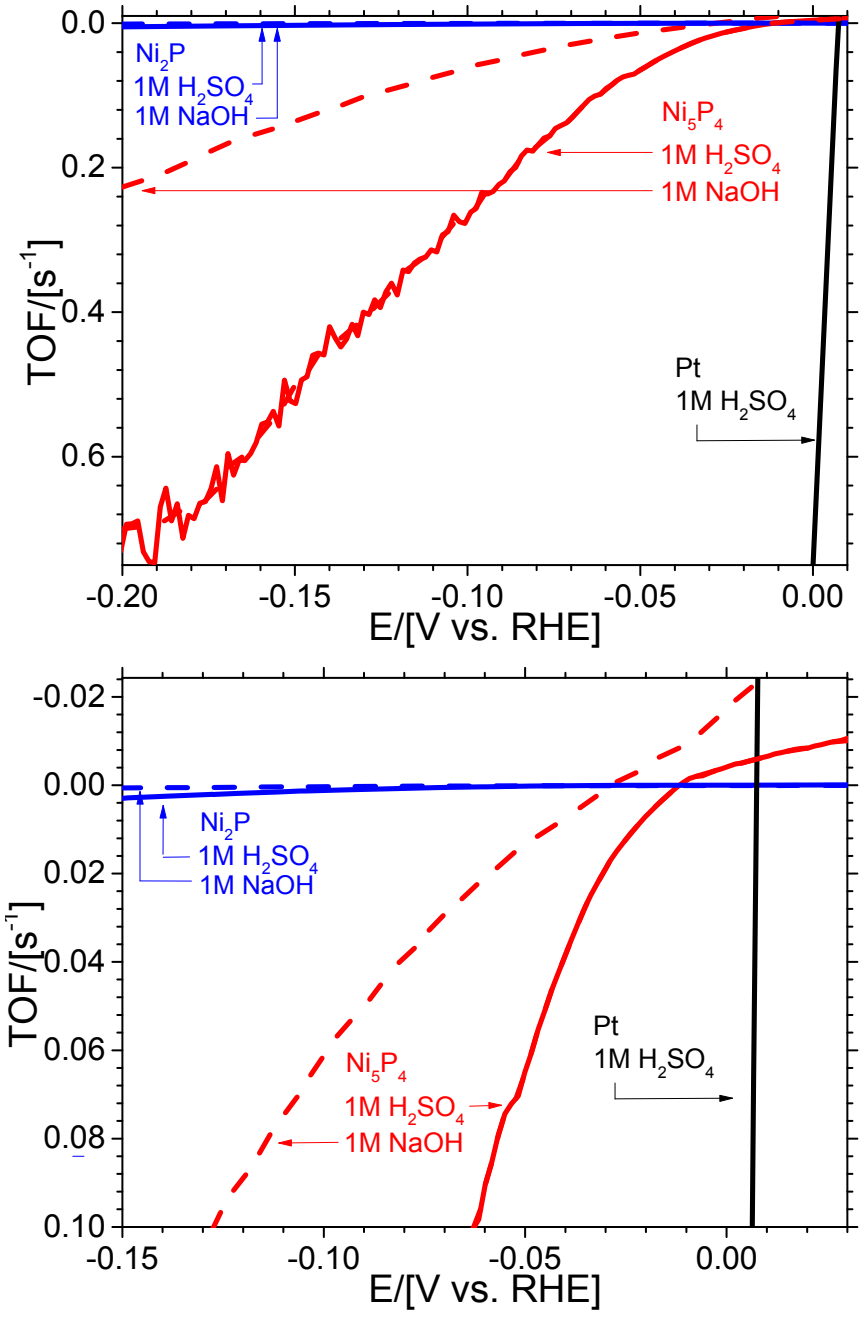

*Fig. S 10 Turn-over frequency (TOF) vs. potential Ni_5P_4 MPs (**red**), Ni_2P NPs (**blue**), and Pt (**black**) in 1 M H_2SO_4 (solid line) and 1 M NaOH (dashed line).*

Popczun et al. [4] estimates the TOF for their material with a 1 mg/cm^2 loading in 0.5 M H_2SO_4 at 100 and 200 mV overpotential to be 0.015 s^{-1} and 0.50 s^{-1}, respectively. This should be compared to the $1.17 \cdot 10^{-3}$ s^{-1} and $5.11 \cdot 10^{-3}$ s^{-1} measured here for the pellet electrodes in 1 M H_2SO_4. Assuming that the particle sizes produced in this work is essentially the same as those prepared by Popczun et al. [4], and neglecting a potential effect of pH (1 M vs. 0.5 M H_2SO_4), it may be estimated that the TOF measured with the estimate of the full thickness of the catalyst pellet being in catalytic contact with the electrolyte introduces an error of 1-2 orders of magnitude. This is a consequence of our conservative estimation of the active electrode surface area based on the assumption that the full depth of the pellet electrode is in contact with the electrolyte. This is highly unlikely—and it is even more unlikely that only the first monolayer of this nanoparticle film is active (6 orders of magnitude higher TOFs would be a consequence)—our estimate is thus a lower bound estimate and this readily explain the 2 order of magnitude difference observed between the data in our study and that of Popzcun et al[4].

Compared to these numbers the Ni_5P_4 MP sample showed a 0.28 s^{-1} and 0.73 s^{-1} at 100 and 200 mV overpotential, respectively in 1 M H_2SO_4. It may be expected that the true TOF of Ni_5P_4 MPs is also 1-2 orders of magnitude larger; due to the previously mentioned approximation of the active surface area.

For reference, the Pt foil electrode show a TOF 329 s^{-1} at 100 mV overpotential in 1 M H_2SO_4. Showing that under the assumption of a completely flat Pt surface every Pt atom does 3-4 orders of magnitude more turn-overs than Pt. At low overpotentials in Fig. S 8 (lower) it would appear that the Pt HER TOF is significant at E >0 V vs RHE, this is an artifact of the low sampling rate in the fast scan rate CV and not attributable to a real HER TOF at these potentials.

Based on the TOFs estimated in this work, the Ni_5P_4 sample performs approximately 3–4 orders of magnitude lower than Pt at low overpotentials. This discrepancy could in part be attributed to: 1. The lower bound estimate of the surface area (the full pellet thickness, or approx. $1.21 \cdot 10^6$ atomic layers (*vide infra*) should be active) and 2. Possibly a poorer conduction through the Ni_5P_4 compared to that of the metallic Pt electrode. If the deviation between the reported values for Ni_2P in the work by Popzcun et al.[4] and our data is applied to the Ni_5P_4 sample, this sample could perform approximately on 1–2 orders of magnitude lower than for Pt. Further studies in our group is directed at determining the accurate TOF for the Ni_5P_4 MPs.

Under alkaline conditions NiMo alloy NPs are the state of the art catalysts. This alloy shows a TOF of 0.05 s^{-1} and 0.36 s^{-1} at 100 mV and 200 mV overpotential, respectively. Popczun et al.[4] do not however report the TOF of their Ni_2P in alkaline conditions. Here the Ni_2P has a TOF of $3.18 \cdot 10^{-4}$ s^{-1} and $1.10 \cdot 10^{-3}$ s^{-1} at 100 mV and 200 mV overpotential, respectively. The NiMo alloy is thus about 2 orders of magnitude better than the Ni_2P. Even under our lower limit estimate Ni_5P_4 MPs performs slightly better than the NiMo alloy NPs, assuming that the Ni_5P_4 MPs active area is actually 1-2 orders of magnitude, as indicated by the comparison for Ni_2P, the Ni_5P_4 would perform 1-2 orders of magnitude better than NiMo alloy NPs.

The above discussed TOFs are summarized in Table S 4 below.

Table S 4 Summary of estimated TOF for nickel phosphide materials, NiMo, Pt and Pt/C.

Catalyst	**TOF/[s^{-1}]** pH 0		**TOF/[s^{-1}]** pH 14		**Reference**
	η = 100 mV	η = 200 mV	η = 100 mV	η = 200 mV	
Ni_5P_4 MP pellet	0.28	0.73	0.063	0.23	This work
Ni_2P NP pellet	$1.17 \cdot 10^{-3}$	$5.11 \cdot 10^{-3}$	$3.18 \cdot 10^{-4}$	$1.10 \cdot 10^{-3}$	This work
10 wt% Pt/C/Nafion	13.5	32.1	4.7	13.7	This work
Bulk Pt	329	N/A	3.6	15.8	This work
NiMo NPs	N/A	N/A	0.05	0.36	[4]
Ni_2P NPs/Ti-foil	0.015	0.5	N/A	N/A	[4]

Turn-over number analysis

Using the approach described above for the CP measurements the number of turnovers completed during the CP analysis could be estimated. Fig. S 11 shows the required potential to draw -10 mA/cm^2 current density vs. turn-over number TON for each material. Due to the very low loading of Pt (approximated as 1 monolayer), this sample far exceeds the TON of both Ni-P phases.

The Ni_5P_4 MP samples performs around 530 turn-overs in the 16 hr reaction time. The Ni_2P NPs has a far greater surface area than the Ni_5P_4 MPs and thus performs very few turn-overs (7 turn-overs).

The very high TON for Ni_5P_4 MPs after 16 hr of H_2 evolution indicates the stability of this material, even under the assumption that the full pellet thickness underneath the exposed surface is electrochemically active.

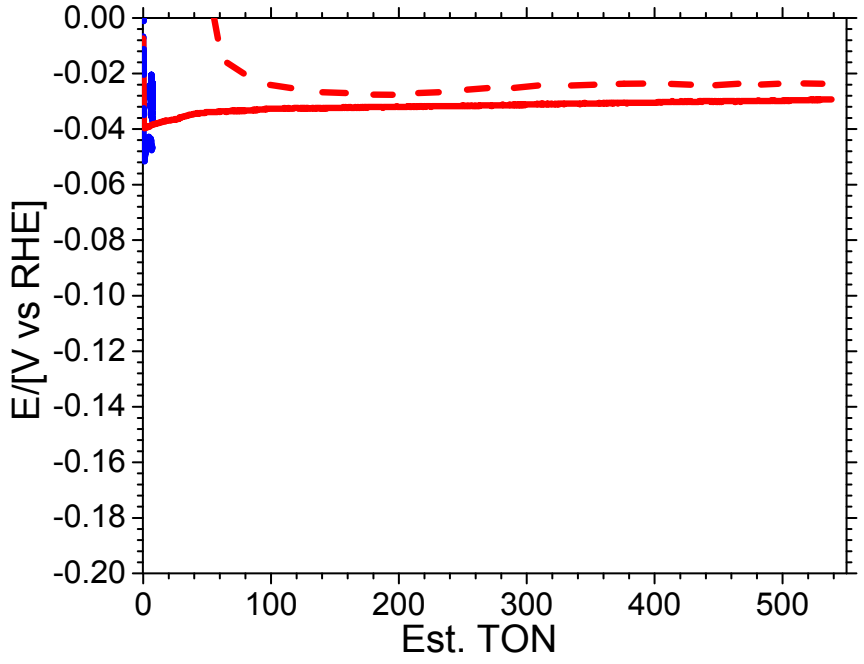

*Fig. S 11 Constant current analysis as a function of TON of Ni_5P_4 MPs (**red**) and Ni_2P NPs (**blue**) in 1 M H_2SO_4 (solid line) and 1 M NaOH (dashed line).*

Electrode thickness estimation

To evaluate the approximate thickness of the pressed pellets in terms of number of atom layers it is assumed that the pellet is completely dense, and that the 36 atoms in the Ni_5P_4 unit cell with volume $438.51 \cdot 10^6$ pm^3 is distributed evenly in a cubic cell as assumed in the TOF analysis above.

It thus follows that:

$$l_{\frac{atoms}{unit\ cell\ height}} = \left(\frac{36\ atoms}{438.51 \cdot 10^{-24} cm^3}\right)^{1/3} = 4.35 \cdot 10^7 atoms/cm$$

$$pellet\ height\ h = \frac{V_{catalyst}}{geometric\ area} = \left(\frac{50mg}{(0.3cm)^2 \cdot \pi}\right) \cdot geometric\ area \cdot \frac{\frac{1}{\rho_{Ni_5P_4}}}{geometric\ area}$$

$$= \left(\frac{50mg}{(0.3cm)^2 \cdot \pi}\right) \Big/ \rho_{Ni_5P_4} = 0.028\ cm$$

$$N_{atom\ layers\ in\ pellet} = 4.35 \cdot 10^7\ {atoms}/{cm} \cdot 0.028cm = 1.21 \cdot 10^6 atoms$$

Active site comparison for Ni_5P_4 and Ni_2P

The active site for the HER on Ni_2P was suggested based on DFT calculations on the [001] facet[12]. Here we will discuss the structural differences for Ni_5P_4 and Ni_2P and rationalize the difference in activity based on this.

Fig. S 12(A) show the Ni_2P [001] facet based the PXRD structure[13] with the Ni_3P_2 termination described in the DFT study (a Ni_3P termination also exists). On each corner of the unit cell there is a triangle of Ni and the subsurface P that according to the DFT calculations forms the active site where the first H^+ is bound at the first electron transfer. This H has a partial negative charge and is therefore termed the hydride from here on (and the corresponding site the hydride site). According to the DFT calculations the second H^+ binds in a bridging position on a nearby Ni-P bond. The latter H is slightly positively charged and H_2 is suggested to form due to electrostatic interaction. The nearest P outside the hydride site lies within this plane and the measured Ni-P distance is 2.209 Å. The authors suggest that the weak binding energy of the second H^+ is the rate limiting step and that a stronger binding of the second proton would lower the barrier for H_2 formation.

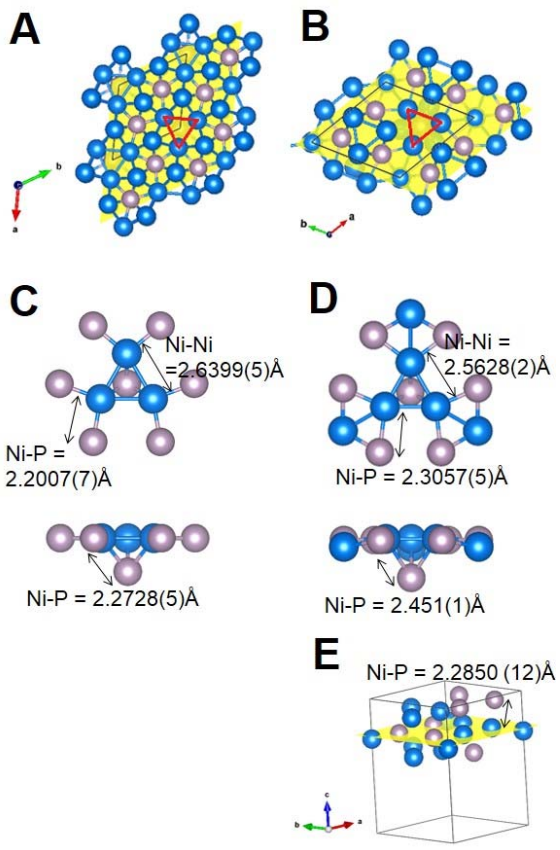

Fig. S 12 Crystal structure of (A) Ni_2P and (B and C) Ni_5P_4, with unit cell marked in black (blue sphere Ni, purple sphere P. (A) shows the Ni_2P [001] facet, with Ni_3P_2 termination. This facet 1 Ni triangle in each corner (marked in red). The yellow plane divides the surface from the subsurface. The subsurface P in the subsurface is the hydride binding site. (B) Shows the Ni_5P_4 [001] facet cut off to expose Ni triangles with subsurface P (marked in red). This is expected to present the hydride site based on the analogy to Ni_2P. (C) And (D) how the extracted active site with Ni-Ni and Ni-P distances. (E) Show the side view of the Ni_5P_4 including the P atoms atop the Ni triangles. Structures are drawn using VESTA 3 software[14] using ICCD references [15,13].

The Ni_5P_4 unit is more complex and consists of two identical cells repeated in the c direction but one is rotated 180°. Fig. S 12C (from PXRD reference [15]) shows the [001] facet of Ni_5P_4; as Ni_5P_4 has multiple potential terminations one is chosen which show the Ni triangles and a surface P structure seen in Ni_2P (for simplicity the cell is truncated at c=[0.55;0.75], see Fig. S 12E). It should be noted that other Ni triangles are seen in the structure, however, these do not have P in the subsurface below the triangle and are therefore disregarded. A yellow plane indicates the division of the surface Ni-triangles and the sub-surface P. For Ni_5P_4 there are 2 possible positions for the second H^+ to bind. One is in the plane of the Ni triangles there are two P per Ni at a distance of 2.306 Å (Fig. S 12D); in addition there is a P above the Ni corners 2.285 Å away (see Fig. S 12(E)). Which of these two sites would be protonated during the HER depends both on the actual facet termination and the H^+ binding energy, which could not be determined from this structural examination. More detailed theoretical and experimental studies are therefore required to determine the exact mechanism of catalysis. In the following we shall assume that the surface is flat and thus the Ni-P participating in the reaction is in the surface plane with a Ni-P bond distance of 2.306 Å.

This suggests that the Ni-P bond, accepting the second H^+, has a bond length that is approximately 0.105 Å longer in the Ni_5P_4 than in Ni_2P. The weaker Ni-P bond would allow for a more ionic character on Ni and P and increase the potential for orbital overlap with the incoming proton—lowering the energy of the rate-determining step, and thus proceed more readily. Further studies are underway correlating this effect for the other low temperature Ni-P phases.

HRTEM and SEM investigation

Fig. S 13 below shows two low resolution TEM images obtained for a sample of as-prepared Ni_5P_4 NPs.

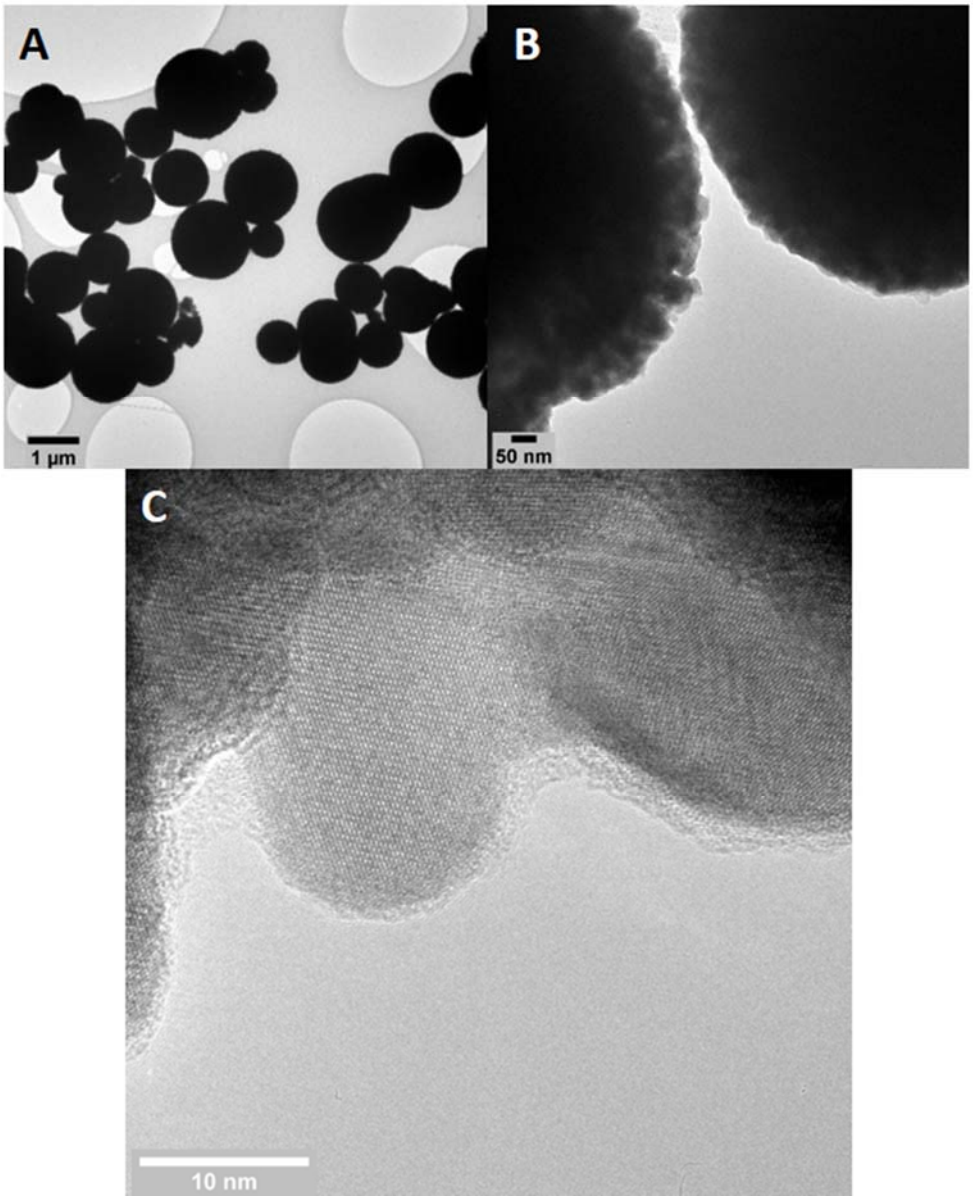

Fig. S 13 A low, B intermediate, and C high resolution TEM images of the Ni_5P_4 NPs after synthesis.

From the low resolution TEM images in Fig. S 13A it could be seen that the Ni_5P_4 sample consist mainly of non-porous spherical particles ranging from 0.3–1.8 µm with the largest fraction being from 1 to 2µm. The observed size range is corroborated by the measured N_2 BET surface area which is <1 m^2/g,

corresponding to an average 949 nm spherical particle. At the intermediate and high magnification Fig. S 13B & C, respectively the spherical particles may be seen to consist of monophasic sintered NPs ranging from 3–86nm in size—the sintering is attributed to the high reaction temperature ~330°C. Most of these nanometer sized particles have a rectangular shape but the smallest are less uniformly shaped. The individual sintered NPs show only one domain of lattice spacing indicating that they are monophasic single crystals.

Representative HRTEM images from both the Ni_5P_4 samples tested in 1 M H_2SO_4 and 1 M NaOH are shown in Fig. S 14 below. From the HRTEM images it may be seen that the particles show lattice planes that extend to the particle surface. This is evidence that no amorphorization of the particle surface has occurred. The particles still show the approximately 1 nm low contrast amorphous C shell after reaction, this further proves that the surface has not changed during catalysis.

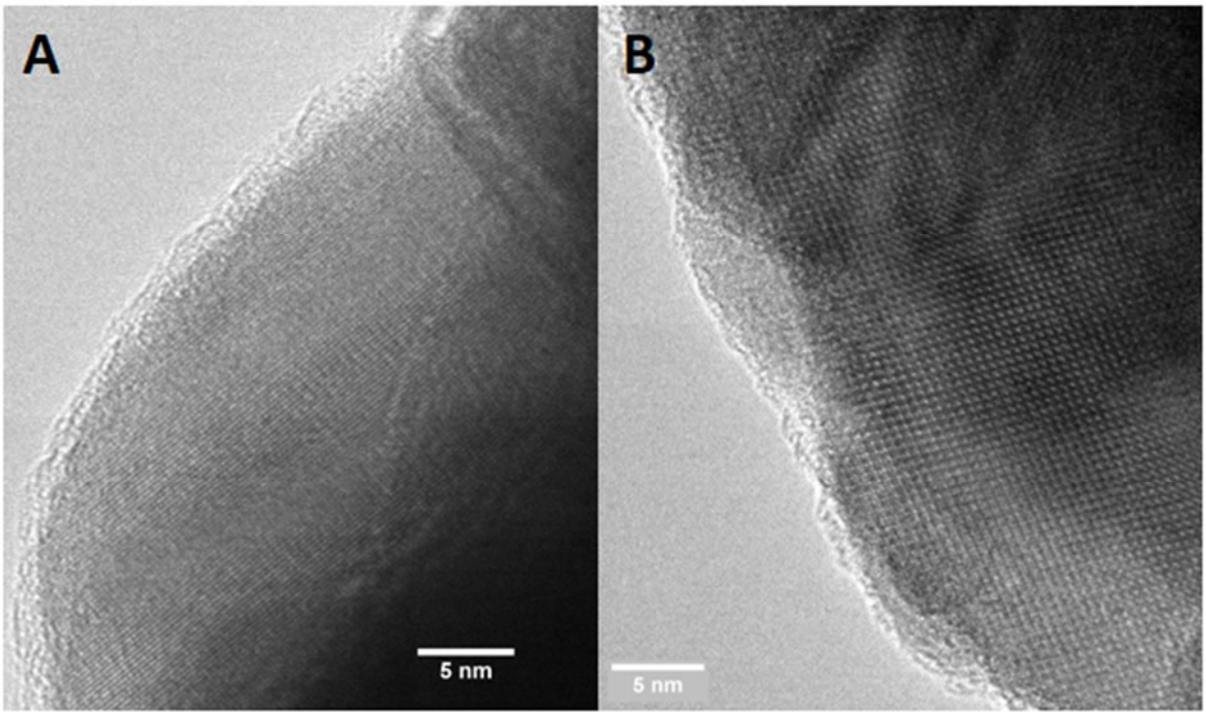

Fig. S 14 HRTEM after 6 hr CP in (A) 1 M H_2SO_4 and (B) 1 M NaOH.

The SEM images in Fig. S 15 below for the Ni_5P_4 samples run for 6 hr in CP measurements show the same size range as observed in HRTEM from less than 0.5 µm to about 2 µm. More interestingly the particles show little difference in size in either acidic or alkaline conditions. This strongly suggests that the particles do not dissolve or change significantly during HER activity. This is also seen from SEM-EDXS measurements given in Table S 4 below, here the weight percentage of 12 randomly selected areas of particles are analyzed and averaged for the sample run in acid or in base. The excellent agreement between these numbers and the expected Ni/P ratios for Ni_5P_4 provides evidence that there are change in composition due to Ni or P losses during catalysis.

Further evidence of this material's stability is given in Table S 5 below, where the lattice spacing obtained from multiple particles in samples either run at constant current density in 1 M H_2SO_4 or 1 M

NaOH for 6 hr is summarized. The lattice spacing is in good agreement with that predicted by reference PXRD patterns and no other crystal structure of nickel phosphide or phosphate presented as good a match as that of Ni_5P_4. In addition, the lattice spacings obtained from the HRTEM image in Fig. 1B are listed showing that the particles imaged does indeed have the Ni_5P_4 crystal structure in agreement with the PXRD pattern shown in Fig. 1A.

From EDXS (with standards as a reference) and diffraction work, it is indicated that both the sample performing the HER for 6 hr in 1 M NaOH and 1 M H_2SO_4 are very closely resembling the Ni_5P_4 structure. Based on this and the PXRD data presented in the main paper it is concluded that the sample is indeed Ni_5P_4 before and after 6 hr reaction under both acidic and alkaline conditions.

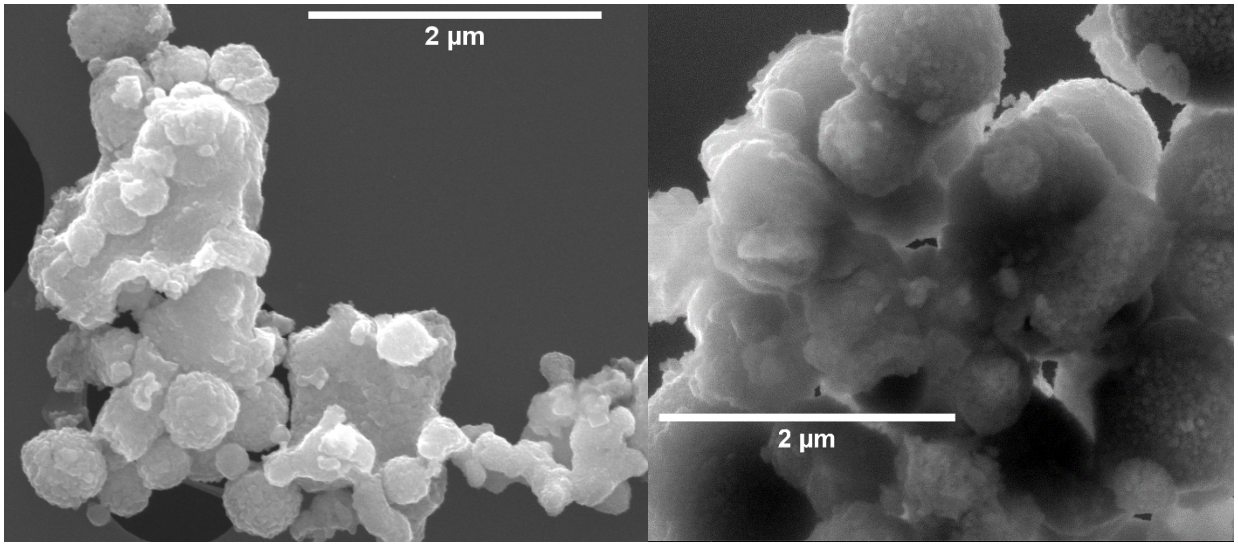

Fig. S 15 SEM images of Ni_5P_4 particles scraped from the electrode surface after 6 hr CP measurement in (left) 1 M H_2SO_4 and (right) 1 M NaOH. The particles appear to have approximately the same morphology and particles size in either electrolyte.

Table S 5 Summary of elemental composition (mass percentages) measured by SEM-EDXS. Column 1 gives the expected ratio for Ni_5P_4. Column 2 & 3 gives the observed ratio averaged over 12 spectra recorded in randomly selected areas on the TEM grid used for HRTEM analysis for a sample run for 6hr in 1 M NaOH or 1 M H_2SO_4, respectively.

Element	**Ni_5P_4 Theoretical**	**Ni_5P_4 (1 M NaOH) Experimental** (12 spectra average)	**Ni_5P_4 (1 M H_2SO_4) Experimental** (12 spectra average)
Ni (mass %)	70	69.36	69.91
P (mass %)	30	30.63	30.88

Table S 6 Summary of lattice spacing as measured by HRTEM. Column 1 gives the indices for each lattice plane, column 2 the expected d spacing according to pdf 00-018-0883 and 01-089-2588, column 3 the d spacing the pristine sample in Fig. 1B, column 4 the d spacing from several images of a Ni_5P_4 sample run for 6 hr in 1 M NaOH, column 5 the d spacing from several images of a Ni_5P_4 sample run for 6 hr in 1 M H_2SO_4.*

(h k L)	**Theoretical d spacing for Ni_5P_4**	**Experimental d spacing for original sample**	**Experimental d spacing for 6 hr run sample in 1 M NaOH**	**Experimental d spacing for 6 hr run sample in 1 M H_2SO_4**
100	5.88		5.86	5.87
002	5.49			5.50
101*	5.18		5.14	4.78
102	4.01	4.01	4.06	4.08
110	3.40		3.39	3.30
103	3.11		3.15	
200	2.94			2.93
112	2.89			
201	2.84	2.84	2.81	

Precautions against Pt contaminants

Pt contaminants were rigorously avoided during the catalytic testing by:

1. Using a non-Pt counter electrode (there was no Pt component used during electrocatalytic measurements on nickel phosphides).
2. Cleaning the cell thoroughly in *aqua regia* and then *piranha* after experiments using Pt as the working electrode.
3. As a further precaution, when Pt was used as the working electrode we avoided oxidizing potentials, thus precluding the possibility of Pt corrosion.
4. We used a two-compartment electrochemical cell fitted with a glass frit between working- and counter-compartments, which restrict the diffusion of any species from the anode chamber to the cathode working electrode.
5. Furthermore, replicated samples were never run in the same order and no variation was found in any of the nickel phosphide replicates depending on whether they were run before or after comparison to the Pt-foil working electrode.

To verify that no significant contamination of the pellet surface had indeed occurred we used SEM-EDXS measurements of the Ni_5P_4 MP samples after 6hr of CP analysis.. A representative EDXS spectrum, out of 12 on each sample, is shown in Fig. S 16 below. Pt has two transitions in the window of analysis Lα = 9.441 keV and Mα = 2.048 keV, however, as the latter overlaps with the Kα = 2.013 keV of P this cannot be used for identification at low concentrations. The 9.441 keV line, on the other hand, is completely absent demonstrating that no Pt is detected in the agglomerate of surface particles after 6 hr of electrolysis — within the ~1wt% detection limit of EDXS. To maximize the surface sensitivity we analyzed only particle agglomerates collected from the surface of the pellet. This effectively increases the detection limit as any material not exposed to electrolyte is not analyzed..

It should be noted that Fe, Co, and Cu are also observed in the EDXS spectrum, these signals originates from the instrument and the Cu TEM grid supporting the sample.

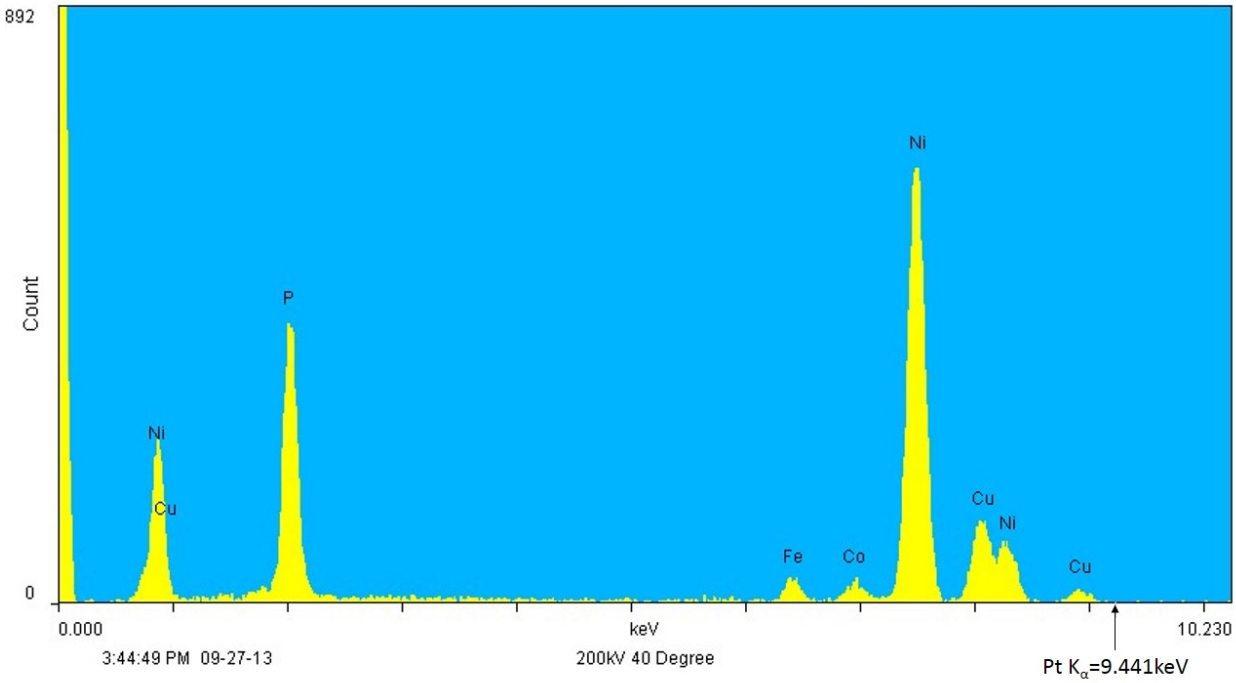

Fig. S 16 Representative SEM-EDXS spectrum of Ni_5P_4 MP electrode surface particles after CP testing for 6 hr in 1 M H_2SO_4.

References

1. K. Aso, A. Hayashi, and M. Tatsumisago, *Inorg. Chem.*, 2011, **50**, 10820–10824.

2. E. Muthuswamy, G. H. L. Savithra, and S. L. Brock, *ACS Nano*, 2011, **5**, 2402–2411.

3. W. Sheng, H. A. Gasteiger, and Y. Shao-Horn, *J. Electrochem. Soc.*, 2010, **157**, B1529.

4. E. J. Popczun, J. R. McKone, C. G. Read, A. J. Biacchi, A. M. Wiltrout, N. S. Lewis, and R. E. Schaak, *J. Am. Chem. Soc.*, 2013, **135**, 9267–70.

5. L. Feng, H. Vrubel, M. Bensimon, and X. Hu, *Phys. Chem. Chem. Phys.*, 2014, **16**, 5917–21.

6. H. M. Rietveld, *J. Appl. Crystallogr.*, 1969, **2**, 65–71.

7. J. Rodríguez-Carvajal, *Phys. B Condens. Matter*, 1993, **192**, 55–69.

8. J. Rodríguez-Carvaja, in *Laboratoire Léon Brillouin (CEA-CNRS), CEA/Saclay, August 24*, 2003.

9. M. Casas-Cabanas, J. Rodríguez-Carvajal, J. Canales-Vázquez, Y. Laligant, P. Lacorre, and M. R. Palacín, *J. Power Sources*, 2007, **174**, 414–420.

10. A. J. Bard and L. R. Faulkner, *Electrochemical Methods: Fundamentals and Applications, Second Edition*, Danvers, 2nd edn., 2000.

11. J. R. McKone, B. F. Sadtler, C. A. Werlang, N. S. Lewis, and H. B. Gray, *ACS Catal.*, 2012, **3**, 166–169.

12. P. Liu and J. A. Rodriguez, *J. Am. Chem. Soc.*, 2005, **127**, 14871–14878.

13. H. N. Nowothy and E. Henglein, *Zeitschrift für Phys. Chemie*, 1938, **40**, 281–284.

14. K. Momma and F. Izumi, *J. Appl. Crystallogr.*, 2011, **44**, 1272–1276.

15. M. Zelinska, S. Oryshchyn, O. Zhak, J. Y. Pivan, M. Potel, and H. Noël, *Acta Crystallogr. E*, 2007, **63**, 158–159.